

Partial Amelioration of Synaptic and Cognitive Deficits by Inhibiting Cofilin Dephosphorylation in an Animal Model of Alzheimer's Disease

Yulei Deng^{a,b}, Jing Wei^{a,c}, Jia Cheng^a, Ping Zhong^{a,c}, Zhe Xiong^a, Aiyi Liu^a, Lin Lin^a, Shengdi Chen^{b,*} and Zhen Yan^{a,c,*}

^a*Department of Physiology & Biophysics, State University of New York at Buffalo, Buffalo, NY, USA*

^b*Department of Neurology & Institute of Neurology, Ruijin Hospital affiliated to Shanghai Jiao Tong University School of Medicine, Shanghai, China*

^c*VA Western New York Healthcare System, Buffalo, NY, USA*

Accepted 10 May 2016

Abstract. The loss of synaptic structure and function has been linked to the cognitive impairment of Alzheimer's disease (AD). Dysregulation of the actin cytoskeleton, which plays a key role in regulating the integrity of synapses and the transport of synaptic proteins, has been suggested to contribute to the pathology of AD. In this study, we found that glutamate receptor surface expression and synaptic function in frontal cortical neurons were significantly diminished in a familial AD (FAD) model, which was correlated with the reduction of phosphorylated cofilin, a key protein regulating the dynamics of actin filaments. Injecting a cofilin dephosphorylation inhibitory peptide to FAD mice led to the partial rescue of the surface expression of AMPA and NMDA receptor subunits, as well as the partial restoration of AMPAR- and NMDAR-mediated synaptic currents. Moreover, the impaired working memory and novel object recognition memory in FAD mice were partially ameliorated by injections of the cofilin dephosphorylation inhibitory peptide. These results suggest that targeting the cofilin-actin signaling holds promise to mitigate the physiological and behavioral abnormality in AD.

Keywords: Actin, Alzheimer's disease, cofilin, glutamate receptors, novel object recognition memory, prefrontal cortex, working memory

INTRODUCTION

Alzheimer's disease (AD) is a devastating neurodegenerative disease commonly found in the elderly population. Diminished synaptic connectivity and

function are believed to be a major contributor to the impaired perception and cognition that characterizes AD [1–3]. Structural and functional impairments in synapses occur at the early stage of AD, and the degree of memory impairment in AD patients correlates well with the extent of synaptic losses, but not with neuronal death [1].

The dynamic features of neuronal synapses result from cycles of continuous actin polymerization and depolymerization, which involves up to 95% of the total actin at dendritic spines [4]. The actin cytoskeleton provides an essential structural support

*Correspondence to: Zhen Yan, PhD, Department of Physiology and Biophysics, School of Medicine and Biomedical Sciences, State University of New York at Buffalo, 124 Sherman Hall, Buffalo, NY 14214, USA. E-mail: zhenyan@buffalo.edu. and Shengdi Chen, MD, Department of Neurology & Institute of Neurology, Ruijin Hospital, Shanghai, 200025, China. E-mail: chen_sd@medmail.com.cn.

for long-term synapse maintenance. The presynaptic filamentous actin (F-actin) meshwork acts as a scaffold to organize the neurotransmitter release machinery, tethering regulators near releasing sites and facilitating vesicle trafficking [5, 6]. Postsynaptic F-actin supports the integrity of dendritic spines, controlling the transport of receptor channels and organizing signaling machinery at the postsynaptic density [5].

Alterations in the organization and dynamics of actin cytoskeleton initiated by filament severing proteins in the ADF/cofilin family have been suggested to link to the synaptic impairment in AD [7]. In neurons under stress, cofilin undergoes activation (dephosphorylation) and forms rod-shaped actin filament bundles (rods), where amyloid- β protein precursor accumulates [8, 9]. These cofilin-saturated rods inhibit synaptic protein transport, impair synaptic transmission and plasticity [10–13], which is considered to contribute to the pathology of AD [8, 14–16]. Amyloid- β ($A\beta$) has also been found to induce spine loss through a pathway involving cofilin and calcineurin [17], which correlates with increased levels of cofilin, and decreased levels of the F-actin-stabilizing spine protein drebrin [18]. Thus, preventing the actin-associated synapse loss represents a major therapeutic strategy for AD treatment.

In this study, we examined the role of actin dysregulation in synaptic deficits of frontal cortex using a familial AD (FAD) model, and explored the potential to ameliorate the physiological and behavioral abnormality in AD by targeting the cofilin-actin signaling.

MATERIALS AND METHODS

Animals

All experiments were performed with the approval of State University of New York at Buffalo Animal Care Committee. The transgenic mice carrying 5 familial AD mutations on human amyloid precursor protein (APP, K670N/M671L + I716V + V717I) and human presenilin 1 (PS1, M146L + L286V), 5 \times FAD, were a generous gift from Dr. William E. Van Nostrand (Stony Brook University). Genotyping were performed by PCR according to the manufacturer's protocol [19, 20].

Primary neuronal culture

Rat cortical cultures were prepared as we previously described [21]. Briefly, frontal cortex was

dissected from Sprague-Dawley rat embryos (E18), and cells were dissociated using trypsin and titrated through a Pasteur pipette. The neurons were plated on coverslips coated with poly-L-lysine in DMEM with 10% fetal calf serum at a density of 5×10^4 cells/cm² or 1×10^6 cells/cm². Low density neuronal cultures were used for immunostaining, while high density neurons were used for biochemical experiments. When neurons attached to the coverslip within 24 hours, the medium was changed to neurobasal media (Invitrogen) with B27 supplement. Cytosine arabinoside (Arac, 5 μ M) was added at DIV3 to stop glial proliferation. Neurons were maintained for 2–3 weeks before being used.

Reagents

The procedure of $A\beta$ oligomer preparation was similar to what was described before [22–24]. In brief, the $A\beta_{1-42}$ peptide (Tocris) was dissolved in hexafluoroisopropanol to 1 mM. Hexafluoroisopropanol was then removed under vacuum. The remaining peptide was then resuspended in DMSO to 5 mM and diluted in H₂O to 0.1 mM. The oligomeric $A\beta$ was formed by incubating at 4°C for 24 h. The TAT-conjugated, phosphorylated cofilin peptide derived from 1–16 residues of cofilin with Ser3 phosphorylation (MAS^PGVAVSDGVKVFN) was designed to act as a cell-permeable inhibitor of endogenous cofilin dephosphorylation (competes for binding to phosphatases) [25–28]. The scrambled TAT peptide or non-phosphorylated cofilin peptide served as negative controls.

Electrophysiological recordings in slices

Standard whole-cell voltage-clamp recordings were used to measure synaptic currents in layer V medial PFC pyramidal neurons as we described previously [27, 29]. Mice were sacrificed after inhaling Halothane (Sigma, St Louis, MO, USA). Brains were immediately removed, iced and cut into 300 μ m slices by a Vibratome (Leica VP1000S, Leica Microsystems Inc., Buffalo Grove, IL, USA). Slices were then incubated in artificial cerebrospinal fluid (ACSF, in mM: 130 NaCl, 26 NaHCO₃, 3 KCl, 5 MgCl₂, 1.25 NaH₂PO₄, 1 CaCl₂, 10 glucose, pH 7.4, 300 mOsm) for 1–6 h at room temperature (20–21°C) bubbling with 95% O₂, 5% CO₂. Prefrontal cortex-containing slices were positioned in a perfusion chamber attached to the fixed stage of an upright microscope (Olympus, Center Valley,

PA, USA) and submerged in continuously flowing oxygenated ACSF. Bicuculline (10 μ M) and CNQX (25 μ M) were added in NMDAR-EPSC recordings. Bicuculline and D-APV (25 μ M) were added in AMPAR-EPSC recordings.

Patch electrodes contained internal solution (in mM): 130 Cs-methanesulfonate, 10 CsCl, 4 NaCl, 10 HEPES (N-2-hydroxyethylpiperazine-N-2-ethane sulfonic acid), 1 MgCl₂, 5 ethylene glycol tetraacetic acid, 2.2 QX-314, 12 phosphocreatine, 5 MgATP, 0.2 Na₂GTP, 0.1 leupeptin, pH 7.2–7.3 and 265–270 mOsm. Cells were visualized with a 40x water-immersion lens and illuminated with near infrared light and the image was detected with an infrared-sensitive CCD camera. A Multiclamp 700 A amplifier was used for these recordings. Tight seals (2–10 G Ω) from visualized neurons were obtained by applying negative pressure. With additional suction, the membrane was disrupted into the whole-cell configuration. Evoked EPSC were generated with a pulse from a stimulation isolation unit controlled by a S48 pulse generator (Astro Med, West Warwick, RI, USA). A bipolar stimulating electrode (FHC, Bowdoinham, ME, USA) was placed \sim 100 μ m from the neuron under recording. Membrane potential was maintained at -70 mV for AMPAR-EPSC recordings. For NMDAR-EPSC, the cell (clamped at -70 mV) was depolarized to $+60$ mV for 3 s before stimulation to fully relieve the voltage-dependent Mg²⁺ block. To obtain the input-output responses, EPSC was elicited by a series of stimulation intensities with the same duration of pulses.

Western blotting

After treatment, slices or cultures were homogenized in boiling 1% SDS. After centrifugation (13,000 \times g, 20 min), the supernatant fractions were subjected to 7.5% or 10% SDS-polyacrylamide gels and transferred to nitrocellulose membranes. The blots were blocked with 5% nonfat dry milk for 1 h at room temperature, followed by incubation with various primary antibodies including anti-cofilin (1:250; Cell Signaling Technology, 2601, or 1:2000; Cell Signaling Technology, 5175), anti-ser³p-cofilin (1:500; Cell Signaling Technology, 3310), anti-LIMK1 (1:500; BD Transduction Laboratories, 611748), anti-p^{T508}LIMK1/ ^{T505}LIMK2 (1:500, Abcam, ab131341), anti-PSD-95 (1:1000; Neuromab, 75-028), anti-tubulin (1:10000; Sigma, T9026), anti-Slingshot (SSH) (1:500; Ecm Bioscience, SP1711) and anti-synaptophysin (1:500;

Chemicon, MAB332). The blots were exposed to the enhanced chemiluminescence substrate (Amersham Biosciences). Quantitation was obtained from densitometric measurements of immunoreactive bands on films.

Biochemical measurement of surface-expressed receptors

The surface NMDA and AMPA receptors were detected as described previously [29, 30]. In brief, after treatment, cortical slices were incubated with ACSF containing 1 mg/ml sulfo-*N*-hydroxysuccinimide- LC-Biotin (Pierce Chemical Co., Rockford, IL) for 20 min on ice. The slices were then rinsed three times in Tris-buffered saline to quench the biotin reaction, followed by homogenization in 300 μ l of modified radioimmunoprecipitation assay buffer (1% Triton X-100, 0.1% SDS, 0.5% deoxycholic acid, 50 mM NaPO₄, 150 mM NaCl, 2 mM EDTA, 50 mM NaF, 10 mM sodium pyrophosphate, 1 mM sodium orthovanadate, 1 mM phenylmethylsulfonyl fluoride, and 1 mg/ml leupeptin). The homogenates were centrifuged at 14,000 \times g for 15 min at 4°C. Protein (15 μ g) was removed to measure total NR1. For surface protein, 150 μ g of protein was incubated with 100 μ l of 50% Neutravidin Agarose (Pierce Chemical Co.) for 2 h at 4°C, and bound proteins were resuspended in 25 μ l of SDS sample buffer and boiled. Quantitative western blots were performed on both total and biotinylated (surface) proteins using anti-NR1 (1:500; Cell signaling, 5704, or 1:500; Neuromab, 75-272), anti-NR2A (1:500; Millipore, 07-632), anti-NR2B (1:500; Millipore, 06600), anti-GluR1 (1:500; Millipore, AB1504), anti-GluR2 (1:500; Neuromab, 75-002), and anti-GABA_A β 3 (1:500; NeuroMab, 75-149).

Synaptosomal fraction and measurement of synaptic proteins

Subcellular fractions were prepared as we described previously [23, 27]. In brief, blocks of frontal cortex were homogenized in ice-cold lysis buffer. 50 μ l of homogenates were saved as the total protein, and the remaining homogenates were subjected to several steps of centrifugation. After centrifugation at 800 \times g for 5 min to remove nuclei and large debris, the remaining supernatant was subjected to 10,000 \times g centrifugation for 10 min. The crude synaptosome fraction (pellet) was suspended in lysis buffer containing 1% Triton X-100 and

300 mM NaCl, homogenized again, and centrifuged at $16,000\times g$ for 30 min to obtain Triton soluble fraction (P1) and Triton insoluble fraction (P2). Triton insoluble fraction which mainly includes membrane-associated proteins from synaptosomes was dissolved in 1% SDS. Samples were boiled in $2\times$ SDS loading buffer for 5 min, and separated on 7.5% SDS-PAGE. Western blots were performed using antibodies against actin (1:1000; Santa Cruz, sc-1616) and PSD-95 (1:1000; Neuromab, 75-028).

Immunocytochemistry

After A β treatment, neurons cultured on coverslips (DIV 14) were fixed in 4% paraformaldehyde in PBS for 20 min at room temperature and washed 3 times with PBS. After permeabilization with 0.1% Triton X-100 in PBS for 20 min, neurons were incubated with 5% bovine serum albumin for 1 h to block nonspecific staining. Next, neurons were incubated with primary antibodies at 4°C overnight, including anti-NeuN (1:1000; Millipore, MAB377) and anti-MAP2 (1:500; Santa Cruz, sc-20172). After washing, neurons were incubated with Alexa Fluor 594-conjugated secondary antibody (1:250, Invitrogen) and Alexa Fluor 488-conjugated secondary antibody (1:250, Invitrogen) for 2 h at room temperature. After washing in PBS for three times, the coverslips were mounted on slides with VECTASHIELD mounting media (Vector Laboratories, Burlingame, CA). Fluorescence images were obtained using a $20\times$ lens and were captured digitally using SPOT basic image capture software. All specimens were imaged under identical conditions and analyzed using identical parameters.

Behavioral tests

Behavioral experimenters were blind to the treatments that animals received. To test working memory, the T-maze delayed alternation task was used as we previously described [31, 32]. Mice (2.5–4 months) were subjected to restricted diet and maintained at approximately 85% of their original weight for 1–2 week. They were habituated to a T-maze until they voluntarily ate a sucrose pellet placed at the end of each arm. T-maze training began only after habituation had finished and when mice showed no visual signs of distress of being in the maze. On the first trial, animals were rewarded for entering either arm. Thereafter, for a total of 11 trials per session, animals were rewarded only if they entered the arm opposite to

the one that was previously chosen. Between trials the choice point was wiped with alcohol to remove olfactory cues. In the initial 1–2 training sessions, the delay between trials started at 5 s, and was subsequently raised in 5-s intervals. In the later training sessions, the delay was fixed at 30 s, and animals were examined daily until establishing baseline performance of 60–70% correct for two consecutive days. The first trial was never included in assessing performance.

Novel object recognition (NOR) task was conducted with minor modifications [33]. The first day of each experiment consisted of 2–3 habituation trials (3 min each, 5 min apart), during which mice explored the arena (44.5 cm in diameter) alone (no objects) in the training room. Twenty-four hours later, the experimental trials began, which consisted of a familiarization phase (phase 1) and a test phase separated by a delay period. During the familiarization phase, mice were placed in the arena containing two copies of an object (A) and allowed to freely explore (3 min per trial). After a short (5 min) delay period, a test trial (3 min) was conducted. Mice were returned to the arena containing one of the original objects (“familiar-A”) and a new, different object (“novel-B”). All objects were made of plastic toys (height: about 5 cm) with similar textures, colors, and sizes, but distinctive shapes. The objects were positioned in two adjacent corners, 10 cm from the walls. The arena and objects were cleaned between each trial with 70% alcohol to mask any olfactory cues. The room was illuminated by indirect white light. Exploration was defined by sniffing or touching the object with the nose. Sitting on the object was not considered exploration. Total exploration time(s) of the familiar and novel objects was recorded and used to calculate a discrimination index (time spent with novel object (B) - time spent with familiar object (A))/(total time exploring both objects (B+A)) for training and test sessions. This index was used to measure recognition memory.

Data analysis

Data analyses were performed with Clampfit (Molecular Devices), Kaleidagraph (Abelbeck/Synergy Software, Reading, PA), Mini Analysis Program (Synaptosoft, Leonia, NJ, USA), and ImageJ software (National Institutes of Health). Experiments with two groups were analyzed statistically using unpaired Student's *t*-tests. Experiments with more than two groups were subjected to one-way ANOVA, followed by *post hoc* Tukey tests.

RESULTS

FAD transgenic mice exhibit the impaired NMDAR and AMPAR surface expression and synaptic currents

To test the potential impairment of excitatory transmission in AD, we examined the expression of NMDAR and AMPAR subunits in FAD mice (2.5-month-old). The prefrontal cortex (PFC), a brain region controlling high-level cognitive processes and exhibiting structural and functional abnormalities at the early stage of AD [34], was mainly used in our studies. We found that the level of surface NMDAR and AMPAR subunits was significantly lower in PFC slices from FAD mice, compared to age-matched wild-type (WT) mice (Fig. 1A, B, NR1: $53.3 \pm 6.3\%$ of WT; NR2A: $53.5 \pm 8.2\%$ of WT; NR2B: $58.8 \pm 8.3\%$ of WT; GluR1: $61.5 \pm 6.1\%$ of WT; GluR2: $56 \pm 6.6\%$ of WT, $n=9$, $p < 0.001$, t -test). In contrast, the level of surface GABA_AR, the major inhibitory receptor in the central nervous system, was not significantly changed (Fig. 1A, B, $n=3$). The level of total NMDAR and AMPAR subunits was not significantly altered in 2.5-month-old FAD mice (Fig. 1A, B, $n=9$). It suggests that FAD mice have the diminished number of glutamate receptors at the plasma membrane.

Next, we compared the NMDAR- and AMPAR-mediated synaptic currents in PFC slices from WT and FAD mice (2.5 months old). As shown in Fig. 2A and B, AMPAR-EPSC and NMDA-EPSC induced by a series of stimulus intensities were markedly reduced in PFC pyramidal neurons from FAD mice, compared to those from WT mice (NMDA: 45%–69% decrease, $n=13$ per group; AMPA: 56%–64% decrease, $n=16$ –21 per group, $p < 0.001$, ANOVA). The loss of cortical NMDAR and AMPAR function in FAD mice may be attributed to the reduced glutamate receptor delivery to the synaptic membrane.

Cofilin phosphorylation and synaptic F-actin are altered in AD conditions

Since the dynamics of actin cytoskeleton plays a key role in regulating NMDAR and AMPAR membrane trafficking [12, 16, 35–37], we examined whether actin regulators were altered in FAD mice. We found that the amount of phosphorylated cofilin was significantly decreased in PFC slices from FAD mice (Fig. 3A, B, $54.2 \pm 6.5\%$ of

WT, $n=8$, $p < 0.01$, t -test), while the total cofilin was unchanged, suggesting that non-phosphorylated cofilin is increased in FAD mice, consistent with the previously reported cofilin hyperactivation in AD patients [7, 8]. The protein level of Slingshot, the phosphatase dephosphorylating and activating cofilin, was not altered in FAD mice (Fig. 3A, B, $n=8$, $p > 0.05$, t -test). LIMK1, the kinase phosphorylating and inactivating cofilin, as well as the phosphorylated and active form of LIMK, p-T⁵⁰⁸LIMK1/T⁵⁰⁵LIMK2, had similar expression in WT and FAD mice (Fig. 3A, B, $n=8$, $p > 0.05$, t -test). No significant changes were observed with the scaffolding protein PSD-95, a postsynaptic marker (Fig. 3A, B, $n=8$, $p > 0.05$, t -test).

Nest, we tested the direct effect of A β ₁₋₄₂ treatment (1 μ M, 7-day) on cofilin and synaptic proteins in cortical cultures. As shown in Fig. 3C and D, phospho-cofilin level was significantly decreased in A β -treated cultures ($75.3 \pm 5.2\%$ of control, $n=7$, $p < 0.01$, t -test), consistent with what we detected in FAD mice, while the protein level of total cofilin was unchanged. No significant change was found on the expression of synaptophysin (a presynaptic marker) and PSD-95 (a postsynaptic marker) with A β treatment (Fig. 3C, D), suggesting that synapses have been maintained. Taken together, these results suggest that cofilin is activated by A β before synapse loss occurs.

To measure cell viability after A β treatment, we performed MAP2 (a dendritic marker) and NeuN (a neuronal nuclear marker) co-staining experiments. Neurons were measured by counting MAP2+/NeuN+ neurons in cortical cultures. As shown in Fig. 3E and F, A β treatment did not significantly alter cell viability, as demonstrated by the normal neuronal density ($p > 0.05$, t -test).

To find out whether the reduced phospho-cofilin in FAD mice may lead to the alteration of actin filaments, we compared the G-actin (Triton-soluble monomeric actin) and F-actin (Triton-insoluble filamentous actin) in the synaptic fraction of frontal cortex from WT versus FAD mice, using the approach similar to what was previously described [27, 38]. We found that the level of total actin or G-actin at the synaptic cytosol (soluble) was largely unchanged, but the level of synaptic F-actin (insoluble) was significantly higher in FAD mice, compared to WT mice (Fig. 3G, H, $80.4\% \pm 19.4\%$ increase, $n=5$ pairs, $p < 0.05$, t -test). The F/G actin ratio was also elevated in FAD mice (Fig. 3G, H, $93.2\% \pm 23.7\%$ increase, $n=5$ pairs, $p < 0.05$, t -test), consistent with

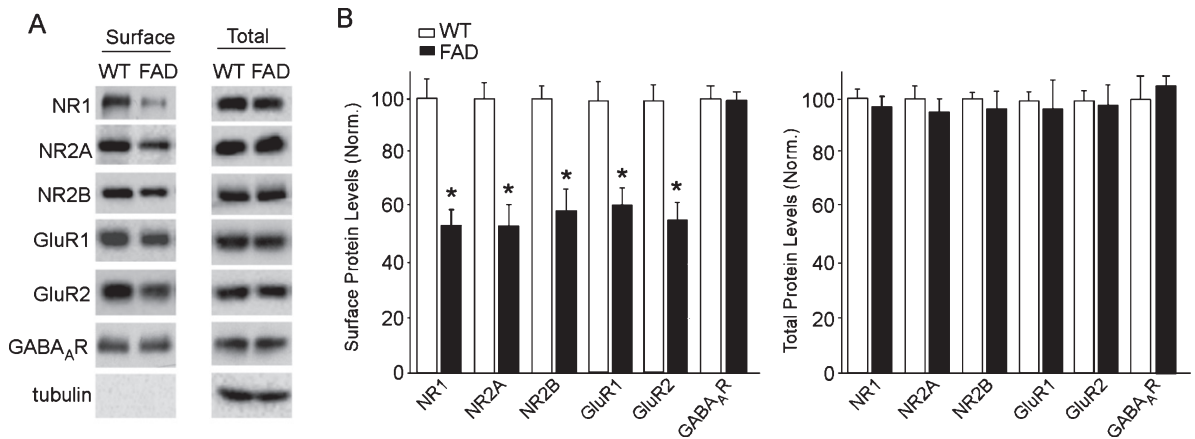


Fig. 1. The surface expression of NMDARs and AMPARs is decreased in frontal cortex of 5xFAD mice. A) Representative western blotting showing the surface and total NR1, NR2A, NR2B, GluR1, GluR2, and GABA_AR β 3 subunits in cortical slices from WT versus FAD mice (2.5-month-old). B) Quantitative analysis of the surface and total level of glutamate receptor subunits and GABA_AR β 3 subunit in FAD mice, compared to WT mice. * $p < 0.001$, t -test.

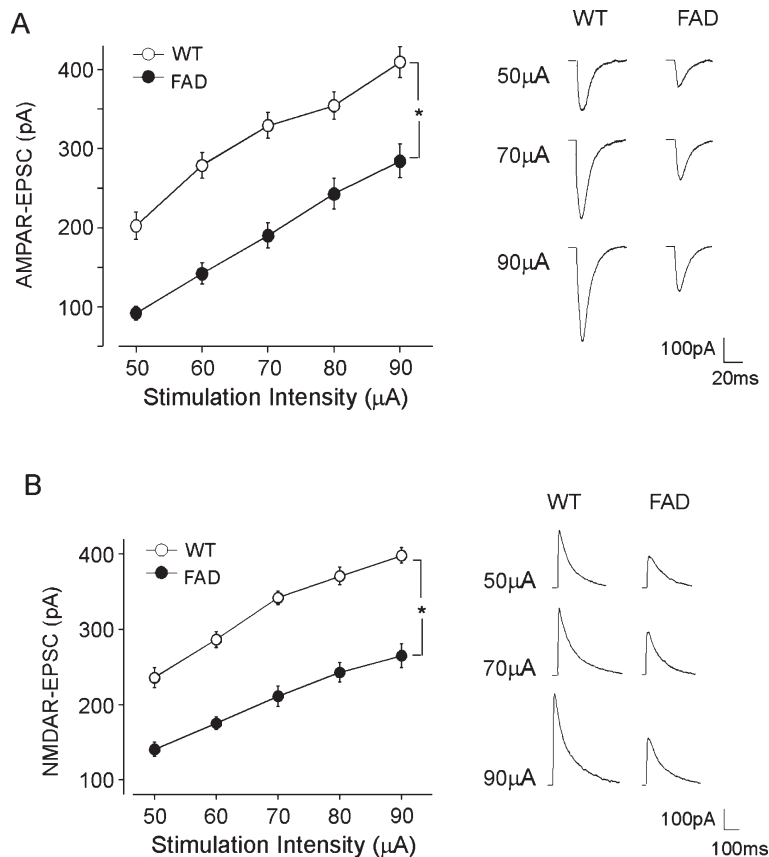


Fig. 2. AMPAR-EPSC and NMDA-EPSC are decreased in PFC pyramidal neurons of 5xFAD mice. A, B) Plot of normalized peak AMPAR-EPSC (A) and NMDAR-EPSC (B) in PFC pyramidal neurons from WT versus FAD mice (2.5-month-old). * $p < 0.001$, ANOVA. Inset: Representative AMPAR-EPSC and NMDAR-EPSC traces.

the A β -induced enhancement of actin polymerization in cultured hippocampal neurons and PC12 cells [39, 40]. In contrast, PSD-95 did not show significant

changes in synaptic fractions. These data suggest that the dynamics of actin filaments is altered in AD.

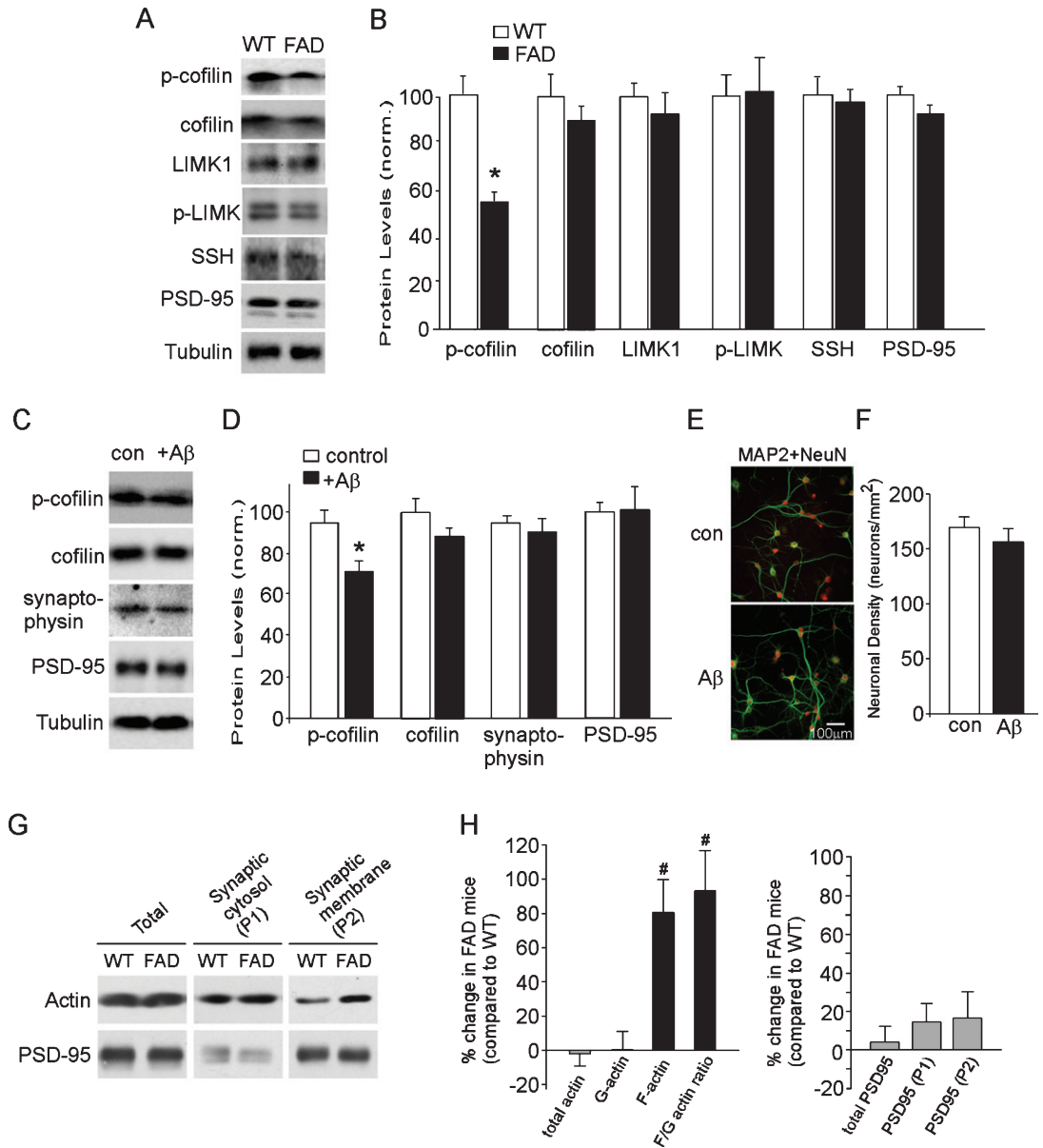


Fig. 3. Phosphorylated cofilin is decreased in 5xFAD mice and Aβ-treated neurons. A, B) Representative western blotting and quantitative analysis of p-cofilin, cofilin, LIMK1, p-LIMK, Slingshot and PSD-95 in cortical slices from WT versus FAD mice (2.5-month-old). * $p < 0.01$, t -test. C, D) Representative western blotting and quantitative analysis of p-cofilin, cofilin, synaptophysin and PSD-95 in cortical cultures without or with Aβ treatment (1 μM, 7 days). Tubulin was used for normalization. * $p < 0.01$, t -test. E, F) Immunocytochemical images and quantitative analysis showing the co-staining of MAP2 (green) and NeuN (red) in cortical cultures without or with Aβ treatment. Scale bars: 100 μm. G, H) Representative western blotting and quantification showing synaptic G-actin (in the Triton-soluble synaptic cytosolic fraction), F-actin (in the Triton-insoluble synaptic membrane fraction) and PSD-95 from PFC of WT versus FAD mice. # $p < 0.05$, t -test.

Inhibiting cofilin dephosphorylation partially rescues synaptic deficits in FAD mice

Given the decreased phospho-cofilin in FAD mice, we tested whether inhibiting cofilin dephosphory-

lation could rescue the synaptic deficits in FAD mice. A peptide consisting of 1–16 residues of Ser3-phosphorylated cofilin was used as an inhibitor of endogenous cofilin dephosphorylation [27, 41, 42]. The p-cofilin peptide is presumed to bind to

endogenous cofilin phosphatases, therefore preventing the dephosphorylation of endogenous cofilin. To render the p-cofilin peptide cell permeable, it was coupled to the protein transduction domain of the human immunodeficiency virus (HIV) TAT protein. Previous studies have demonstrated that systemic injections can reliably deliver TAT peptides into CNS neurons [27, 43, 44]. Thus, we gave i.v. injections of TAT-p-cofilin peptide (10 pmol/g, once daily for 7 days) to animals. As shown in Fig. 4A and B, the systemic administration of TAT-p-cofilin peptide led to a significant increase of endogenous p-cofilin, but not total cofilin, in cortical slices of FAD mice. It suggests that the TAT-p-cofilin peptide indeed inhibits the dephosphorylation of endogenous cofilin in the brain.

Next, we examined NMDAR and AMPAR surface expression after i.v. injections of TAT-p-cofilin peptide (10 pmol/g, 7 days) in FAD mice. As shown in Fig. 4C and D, compared to wild-type mice, the levels of surface NMDAR and AMPAR subunits were significantly diminished in FAD mice injected with TAT control peptide (NR1, $47.8 \pm 1.4\%$ of WT, NR2A: $47.2 \pm 4.6\%$ of WT, NR2B, $51.1 \pm 3.7\%$ of WT, GluR1, $50.1 \pm 6.5\%$ of WT, GluR2, $55 \pm 8.3\%$ of WT, $n=7$), but these surface receptors were partially recovered in FAD mice injected with TAT-p-cofilin peptide (NR1, $67.6 \pm 8.2\%$ of WT; NR2A, $79.1 \pm 5.9\%$ of WT; NR2B, $76.3 \pm 3.8\%$ of WT, GluR1, $83.8 \pm 8.7\%$ of WT; GluR2, $87.9 \pm 4.1\%$ of WT, $n=7$, $p<0.05$, ANOVA, compared to FAD+control peptide). These data suggest that inhibition of cofilin dephosphorylation can result in the partial restoration of glutamate receptor membrane delivery in FAD mice.

We further examined whether AMPAR- and NMDAR-mediated synaptic transmission could be restored in FAD mice after i.v. injections of TAT-p-cofilin peptide (10 pmol/g, 7 days). As shown in Fig. 5A and B, the input/output curves of AMPAR-EPSC and NMDAR-EPSC in PFC pyramidal neurons had partial recovery in FAD mice injected with TAT-p-cofilin peptide (AMPA: 40–80% increase, compared to TAT-injected FAD mice, $n=5$ –10 per group, $n=NMDA$: 35–50% increase, compared to TAT-injected FAD mice, $n=8$ –14 per group, $p<0.05$, ANOVA, FAD+p-cofilin pep. versus FAD+TAT pep.). Neither the AMPAR- nor the NMDAR-mediated synaptic response has completely returned to the level of wild-type animals. Thus, cofilin inhibition can result in the partial recovery of glutamatergic transmission in FAD mice.

Inhibiting cofilin dephosphorylation partially ameliorates cognitive impairment in FAD mice

To determine the functional consequences of inhibiting cofilin dephosphorylation in FAD mice, we examined working memory (WM), a key cognitive process relying on PFC glutamatergic transmission [29, 45, 46], and novel object recognition (NOR) memory, another cognitive process involving PFC [47].

WM was assessed using the T-maze alternation task [31, 32]. A significant reduction of the percentage correctness of choices in the T-maze testing was observed in FAD mice (4-month-old), compared to age-matched WT mice (Fig. 6A, WT: $72 \pm 2\%$, $n=10$; FAD: $48 \pm 2.6\%$, $n=9$, $p<0.01$, ANOVA). Injections with the TAT-p-cofilin peptide partially alleviated the WM deficit in FAD mice, while TAT control peptide or non-phosphorylated cofilin peptide, TAT-cofilin peptide, was ineffective (Fig. 6A, TAT: $50 \pm 2.6\%$, $n=8$; TAT-p-cofilin: $60 \pm 2.3\%$, $n=9$, TAT-cofilin: $47.5 \pm 6.3\%$, $n=4$, $F_{4,39}=23.2$, $p<0.05$, ANOVA).

To determine the influence of cofilin dephosphorylation inhibition in individual FAD mice, we performed T-maze tests on the same mice before and after peptide injections. As shown in Fig. 6B, most of the FAD mice (5/6) had improved WM performance after 7-day TAT-p-cofilin peptide injections, while no improvement was found in FAD mice injected with TAT control peptide ($n=4$).

To further confirm the impact of cofilin inhibition on cognitive functions in FAD mice, we measured the Novel Object Recognition (NOR) task, a fundamental explicit memory process requiring judgments of the prior occurrence of stimuli based on the relative familiarity of individual objects [48, 49]. As shown in Fig. 7A, WT mice (4-month-old) spent much more time exploring the novel object in the test phase (familiar object: 15.9 ± 3.7 s, novel object: 36.7 ± 6.2 s, $n=9$, $p<0.01$, t -test), whereas FAD mice (4-month-old) lost the preference to the novel object (familiar object: 13.4 ± 4.3 s; novel object: 9 ± 2.7 s, $n=7$, $p>0.05$, t -test). After TAT-p-cofilin peptide injections for 7 days, FAD mice showed an increased trend in exploring the novel object (familiar object: 18.3 ± 4.7 s, novel object: 25.5 ± 6.0 s, $n=7$), while injections with control peptides (TAT-peptide or TAT-cofilin peptide) were ineffective (TAT, familiar object: 21.5 ± 4.3 s, novel object: 19.5 ± 3.7 s, $n=7$; TAT-cofilin, familiar object: 17.6 ± 1.3 s, novel object: 11.2 ± 1.3 s, $n=4$). The discrimination index (DI) of NOR task,

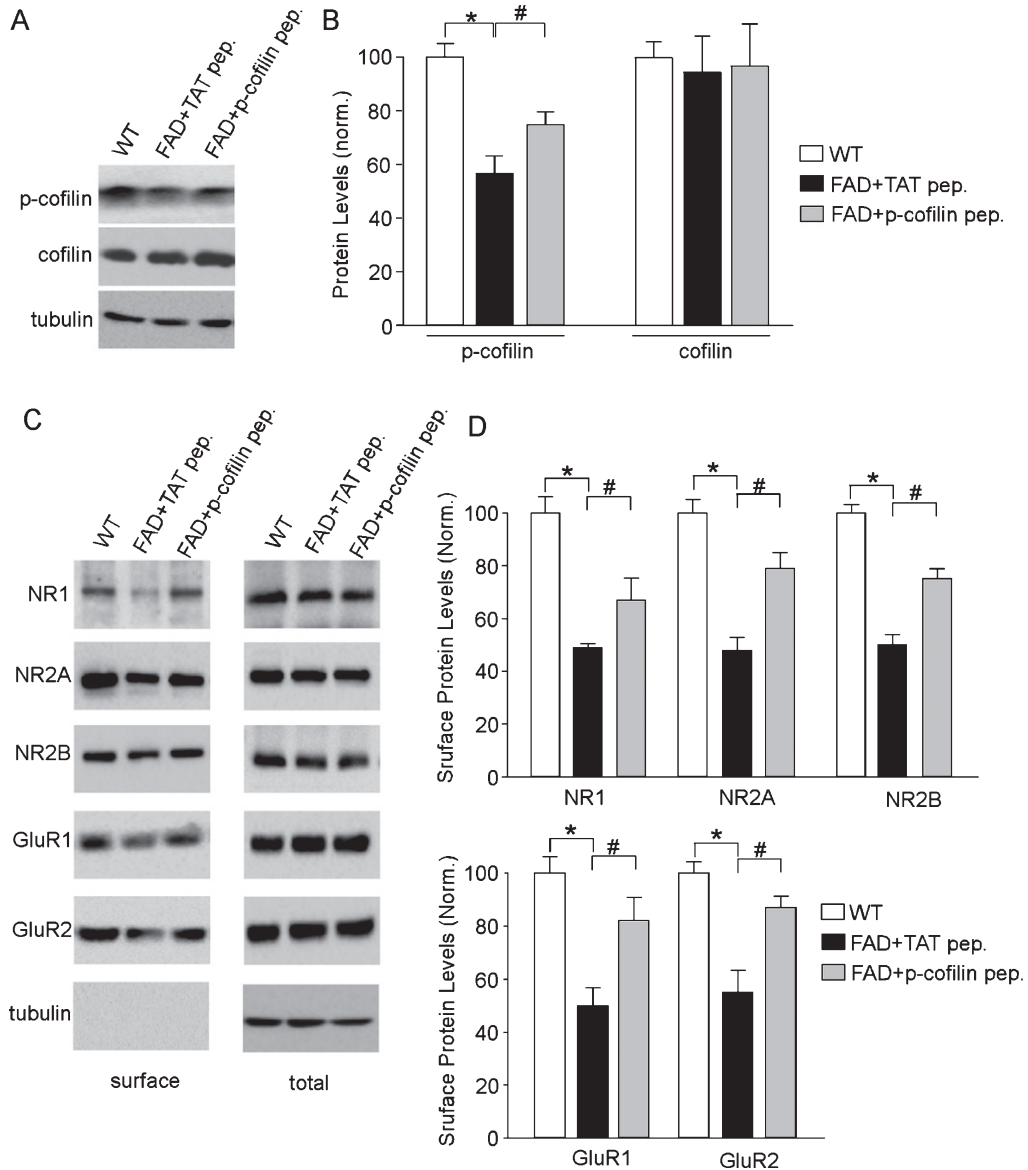


Fig. 4. Inhibiting cofilin dephosphorylation partially recovers the surface expression of NMDARs and AMPARs in 5xFAD mice. A, B) Representative western blotting and quantitative analysis of p-cofilin and cofilin in cortical slices from WT and FAD mice (2.5-month-old) with i.v. injections of TAT-p-cofilin peptide (10 pmol/g, 7 days) or TAT control peptide (10 pmol/g, 7 days). The level of p-cofilin was normalized to total cofilin. The level of total cofilin was normalized to tubulin. * $p < 0.01$, # $p < 0.05$, ANOVA. C, D) Representative western blotting and quantitative analysis of surface and total NR1, NR2A, NR2B, GluR1, and GluR2 subunits in cortical slices from WT or FAD mice with i.v. injections of TAT-p-cofilin peptide or TAT control peptide. * $p < 0.01$, # $p < 0.05$, ANOVA.

which indicates the differential time in exploring the novel versus familiar object, was significantly impaired in FAD mice (Fig. 7B, WT: 0.44 ± 0.08 , $n = 9$, FAD: -0.18 ± 0.02 , $n = 7$; $p < 0.001$, ANOVA). Injecting TAT-p-cofilin peptide to FAD mice led to the partial recovery of NOR recognition memory (Fig. 7B, TAT-p-cofilin: 0.14 ± 0.06 , $n = 7$, TAT: -0.11 ± 0.09 , $n = 7$; TAT-cofilin: -0.23 ± 0.03 , $n = 4$,

$p < 0.05$, ANOVA). These data suggest that inhibition of cofilin dephosphorylation can result in the partial recovery of cognitive functions in FAD mice.

DISCUSSION

A big challenge in the AD field is to understand the causal factors that contribute to the common patholo-

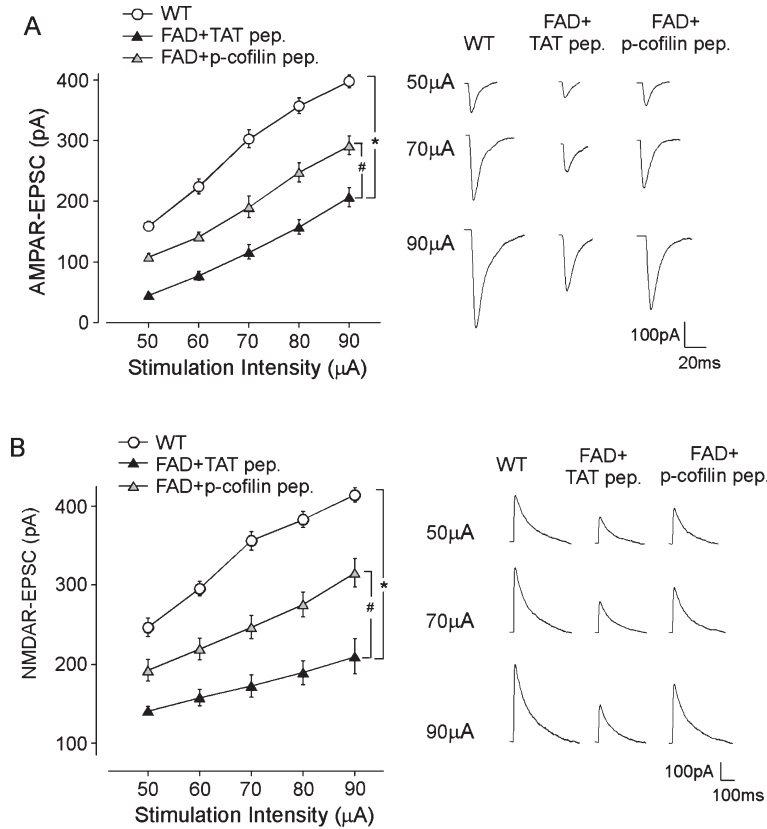


Fig. 5. Inhibiting cofilin dephosphorylation partially restores NMDAR-EPSC and AMPAR-EPSC in 5xFAD mice. A, B) Plot of normalized peak AMPAR-EPSC (A) and NMDAR-EPSC (B) in WT and FAD mice (2.5-month-old) with i.v. injections of TAT-p-cofilin peptide (10 pmol/g, 7 days) or TAT control peptide (10 pmol/g, 7 days). Inset: Representative AMPAR-EPSC and NMDAR-EPSC traces. * $p < 0.01$, # $p < 0.05$, ANOVA.

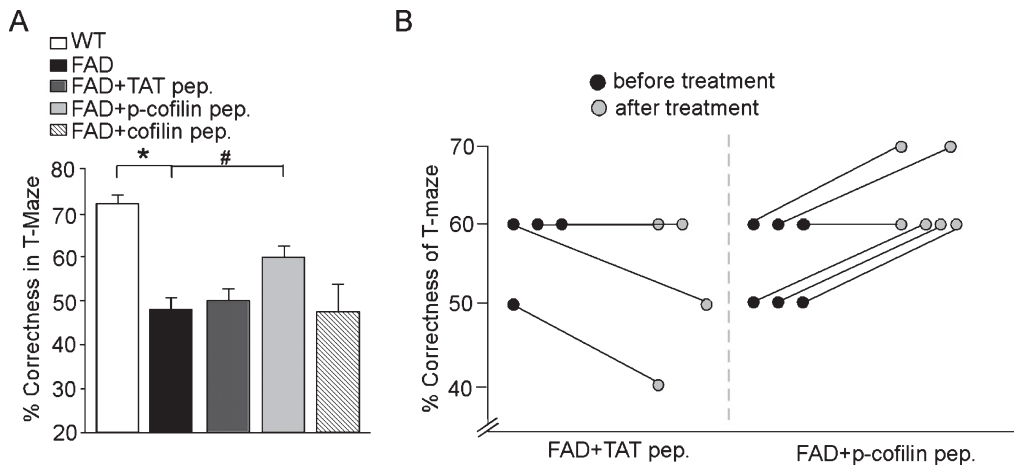


Fig. 6. Inhibiting cofilin dephosphorylation partially ameliorates working memory deficits in 5xFAD mice. A) Bar graphs (mean \pm SEM) showing the percentage correctness in T-maze WM tests in WT and FAD mice (4-month-old) with i.v. injections of TAT-p-cofilin peptide, TAT control peptide or TAT-cofilin-peptide (10 pmol/g, 7 days). * $p < 0.01$, # $p < 0.05$, ANOVA. B) Scatter plots showing the percentage correctness in T-maze tests in each of the tested FAD mice before and after i.v. injections of TAT-p-cofilin or TAT control peptide (10 pmol/g, 7 days).

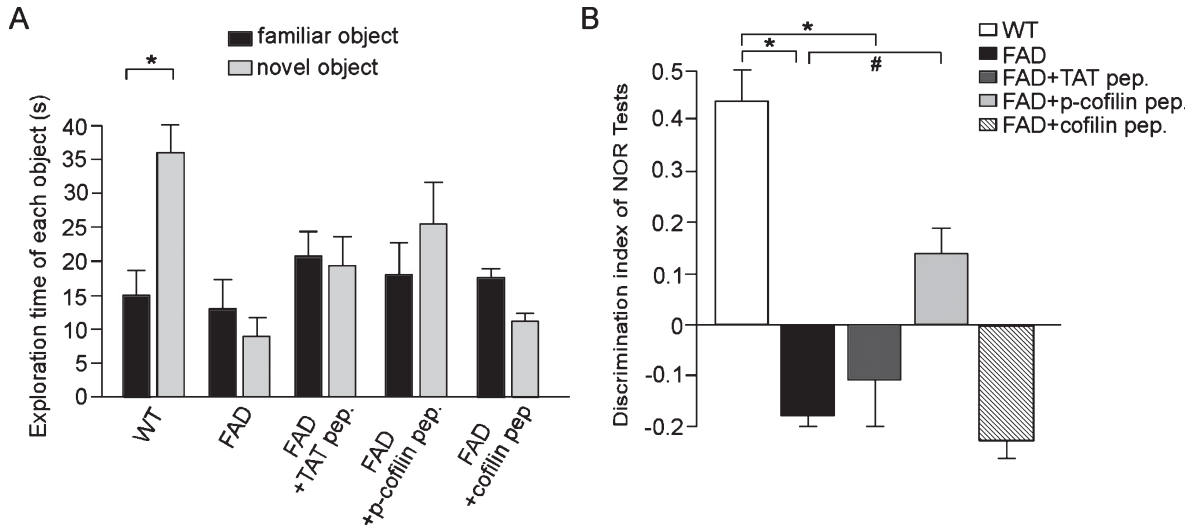


Fig. 7. Inhibiting cofilin dephosphorylation partially restores novel object recognition memory in 5x FAD mice. A) Bar graphs (mean \pm SEM) showing the time of exploring the familiar and the novel object in NOR tests in WT and FAD mice with i.v. injections of TAT-p-cofilin peptide, TAT control peptide or TAT-cofilin peptide (10 pmol/g, 7 days). * $p < 0.01$, t -test. B) Bar graphs showing the discrimination index (DI) of NOR tests in WT and FAD mice with i.v. injections of TAT-p-cofilin peptide, TAT control peptide or TAT-cofilin peptide (10 pmol/g, 7 days). * $p < 0.001$, # $p < 0.05$, ANOVA.

gies found in familial and sporadic AD patients, including the loss of synapses, production of excess A β , and formation of neurofibrillary tangles. It has been suggested that cofilin-actin rods may mediate all these pathological hallmarks of AD, and provide an ideal target for therapeutic intervention [7]. Initiators of neuronal dysfunction and degeneration, such as soluble forms of A β , oxidative stress, mitochondrial dysfunction and excitotoxic glutamate, can stimulate the dephosphorylation of cofilin and the formation of rod-shaped cofilin-saturated actin filament bundles [8]. Cofilin-actin rods in neurites serve as sites of vesicle transport inhibition [9, 13], contributing to the transport defects early in the pathogenesis of AD [16, 50]. Moreover, A β induction of rods potentiates the secretion of A β in a positive loop [9, 51]. Tau-induced neuronal degeneration has also been found to be mediated by abnormal bundling and accumulation of F-actin [15]. All these lines of evidence suggest that manipulating cofilin-actin signaling might be of therapeutic significance for AD and related dementias [52].

Using a familial AD model with the elevated A β burden, we have found impaired synaptic functions at glutamatergic synapses of frontal cortical principal neurons, which is likely attributed to the loss of glutamate receptors at synaptic membrane (Figs. 1 & 2). The delivery and stability of glutamate receptors at synapses are dependent on the dynamics of actin cytoskeleton [12, 27, 42, 53], which is dynam-

ically controlled by cofilin and other actin binding proteins [54, 55]. Correlated with the diminished glutamate receptor surface expression, we have found the decreased level of phosphorylated cofilin in frontal cortex of FAD mice or A β -treated cortical cultures (Fig. 3). Cofilin modulates actin in a self-regulatory manner, with the ability of enhancing F-actin severing and subunit turnover when at low stoichiometry and the ability of binding and stabilizing F-actin at high stoichiometry [54, 56]. The increased synaptic F-actin in PFC of FAD mice (Fig. 3) suggests that the increased level of dephosphorylated cofilin may serve to stabilize F-actin, contributing to the formation of actin rods and the ensuing disruption of glutamate receptor trafficking and function.

How does the elevated A β induce cofilin dephosphorylation in FAD mice? Active cofilin is usually generated by the specific and highly regulated phosphatases in the slingshot family [57]. Although slingshot expression does not show significant changes in FAD mice (Fig. 3), the activity of this phosphatase, which is regulated by phosphorylation and F-actin binding, may be altered in AD. Another potential regulator is the scaffolding protein RanBP9, which mediates cofilin dephosphorylation by slingshot through A β -integrin interactions [58]. It has been found that RanBP9 protein level is significantly increased in brains of AD patients and FAD transgenic mice [58, 59]. Interestingly, recent

studies have demonstrated that the memory deficit in contextual fear conditioning could be improved by blocking cofilin dephosphorylation via lowering RanBP9, and a complete restoration of this fear conditioning response and long-term potentiation in brain slices could be achieved by lowering cofilin levels by 50% [60, 61]. These studies support the notion that cofilin is a potential target for AD treatment.

To test the therapeutic potential of manipulating cofilin-actin signaling, we have administered a cell-permeable cofilin dephosphorylation inhibitory peptide. Interestingly, the surface expression of glutamate receptors and glutamatergic synaptic responses are partially rescued in FAD mice with cofilin dephosphorylation inhibition (Figs. 4 and 5). Corresponding with the synaptic recovery, cognitive deficits in FAD mice, as measured by the working memory test and novel object recognition test, are also partially ameliorated in FAD mice with cofilin dephosphorylation inhibition (Figs. 6 and 7). The incomplete recovery could be due to multiple reasons. First, it is hard to reach the optimal regulation of actin filament dynamics with the cofilin dephosphorylation inhibitory peptide. Second, the cofilin-actin rods are difficult to be completely removed [7]. Third, the limited brain permeability of the cofilin inhibitory peptide may reduce its efficacy in reversing the deficits. Small molecule compounds that have better neuronal accessibility and target specificity are needed. Nevertheless, our results provide the proof-of-concept that targeting cofilin to normalize actin cytoskeleton holds promise to mitigate the physiological and behavioral abnormality in AD.

ACKNOWLEDGMENTS

This work was supported by a VA Merit Award (no. 1I01BX001633) to Z.Y., the National Institutes of Health grants (DA037618, MH108842) to Z.Y., the National Natural Science Foundation of China grants (81300932, 81571029) to S.C and Y. D. We thank Xiaoqing Chen for her excellent technical support.

Authors' disclosures available online (<http://j-alz.com/manuscript-disclosures/16-0167r2>).

REFERENCES

- [1] Terry RD, Masliah E, Salmon DP, Butters N, DeTeresa R, Hill R, Hansen LA, Katzman R (1991) Physical basis of cognitive alterations in Alzheimer's disease: Synapse loss is the major correlate of cognitive impairment. *Ann Neurol* **30**, 572-580.
- [2] Marcello E, Epis R, Saraceno C, Di Luca M (2012) Synaptic dysfunction in Alzheimer's disease. *Adv Exp Med Biol* **970**, 573-601.
- [3] Tu S, Okamoto S, Lipton SA, Xu H (2014) Oligomeric A β -induced synaptic dysfunction in Alzheimer's disease. *Mol Neurodegener* **9**, 48.
- [4] Honkura N, Matsuzaki M, Noguchi J, Ellis-Davies GC, Kasai H (2008) The subspine organization of actin fibers regulates the structure and plasticity of dendritic spines. *Neuron* **57**, 719-729.
- [5] Dillan C, Goda Y (2005) The actin cytoskeleton: Integrating form and function at the synapse. *Annu Rev Neurosci* **28**, 25-55.
- [6] Halpain S (2003) Actin in a supporting role. *Nat Neurosci* **6**, 101-102.
- [7] Bamberg JR, Bernstein BW, Davis RC, Flynn KC, Goldsbury C, Jensen JR, Maloney MT, Marsden IT, Minamide LS, Pak CW, Shaw AE, Whiteman I, Wiggan O (2010) ADF/Cofilin-actin rods in neurodegenerative diseases. *Curr Alzheimer Res* **7**, 241-250.
- [8] Minamide LS, Striegl AM, Boyle JA, Meberg PJ, Bamberg JR (2000) Neurodegenerative stimuli induce persistent ADF/cofilin-actin rods that disrupt distal neurite function. *Nat Cell Biol* **2**, 628-636.
- [9] Maloney MT, Minamide LS, Kinley AW, Boyle JA, Bamberg JR (2005) Betasecretase-cleaved amyloid precursor protein accumulates at actin inclusions induced in neurons by stress or amyloid beta: A feedforward mechanism for Alzheimer's disease. *J Neurosci* **25**, 11313-11321.
- [10] Jang DH1, Han JH, Lee SH, Lee YS, Park H, Lee SH, Kim H, Kaang BK (2005) Cofilin expression induces cofilin-actin rod formation and disrupts synaptic structure and function in Aplysia synapses. *Proc Natl Acad Sci U S A* **102**, 16072-16077.
- [11] Whiteman IT, Gervasio OL, Cullen KM, Guillemin GJ, Jeong EV, Witting PK, Antao ST, Minamide LS, Bamberg JR, Goldsbury C (2009) Activated actin-depolymerizing factor/cofilin sequesters phosphorylated microtubule-associated protein during the assembly of Alzheimer-like neurotic cytoskeletal striations. *J Neurosci* **29**, 12994-13005.
- [12] Gu J, Lee CW, Fan Y, Komlos D, Tang X, Sun C, Yu K, Hartzell HC, Chen G, Bamberg JR, Zheng JQ (2010) ADF/cofilin-mediated actin dynamics regulate AMPA receptor trafficking during synaptic plasticity. *Nat Neurosci* **13**, 1208-1215.
- [13] Cichon J, Sun C, Chen B, Jiang M, Chen XA, Sun Y, Wang Y, Chen G (2012) Cofilin aggregation blocks intracellular trafficking and induces synaptic loss in hippocampal neurons. *J Biol Chem* **287**, 3919-3929.
- [14] Maloney MT, Bamberg JR (2007) Cofilin-mediated neurodegeneration in Alzheimer's disease and other amyloidopathies. *Mol Neurobiol* **35**, 21-44.
- [15] Fulga TA, Elson-Schwab I, Khurana V, Steinhilb ML, Spires TL, Hyman BT, Feany MB (2007) Abnormal bundling and accumulation of F-actin mediates tau-induced neuronal degeneration *in vivo*. *Nat Cell Biol* **9**, 139-148.
- [16] Rust MB (2015) ADF/cofilin: A crucial regulator of synapse physiology and behavior. *Cell Mol Life Sci* **72**, 3521-3529.
- [17] Shankar GM, Bloodgood BL, Townsend M, Walsh DM, Selkoe DJ, Sabatini BL (2007) Natural oligomers of the Alzheimer amyloid-beta protein induce reversible synapse loss by modulating an NMDA-type glutamate receptor-dependent signaling pathway. *J Neurosci* **27**, 2866-2875.
- [18] Zhao L, Ma QL, Calon F, Harris-White ME, Yang F, Lim GP, Morihara T, Ubeda OJ, Ambegaokar S, Hansen JE, Weisbart

- RH, Teter B, Frautschy SA, Cole GM (2006) Role of p21-activated kinase pathway defects in the cognitive deficits of Alzheimer disease. *Nat Neurosci* **9**, 234-242.
- [19] Oakley H, Cole SL, Logan S, Maus E, Shao P, Craft J, Guillozet-Bongaerts A, Ohno M, Disterhoft J, Van Eldik L, Berry R, Vassar R (2006) Intraneuronal beta-amyloid aggregates, neurodegeneration, and neuron loss in transgenic mice with five familial Alzheimer's disease mutations: Potential factors in amyloid plaque formation. *J Neurosci* **26**, 10129-10140.
- [20] Ou-Yang MH, Xu F, Liao MC, Davis J, Robinson JK, Van Nostrand WE (2015) The N-terminal region of myelin basic protein reduces fibrillar amyloid-beta deposition in Tg-5xFAD mice. *Neurobiol Aging* **36**, 801-811.
- [21] Wei J, Graziane NM, Wang H, Zhong P, Wang Q, Liu W, Hayashi-Takagi A, Korth C, Sawa A, Brandon NJ, Yan Z (2014) Regulation of N-methyl-D-aspartate receptors by disrupted-in-schizophrenia-1. *Biol Psychiatry* **75**, 414-424.
- [22] Dahlgren KN, Manelli AM, Stine WB Jr, Baker LK, Krafft GA, LaDu MJ (2002) Oligomeric and fibrillar species of amyloid-beta peptides differentially affect neuronal viability. *J Biol Chem* **277**, 32046-32053.
- [23] Gu Z, Liu W, Yan Z (2009) {beta}-Amyloid impairs AMPA receptor trafficking and function by reducing Ca²⁺/calmodulin-dependent protein kinase II synaptic distribution. *J Biol Chem* **284**, 10639-10649.
- [24] Liu W, Dou F, Feng J, Yan Z (2011) RACK1 is involved in β -amyloid impairment of muscarinic regulation of GABAergic transmission. *Neurobiol Aging* **32**, 1818-1826.
- [25] Aizawa H, Wakatsuki S, Ishii A, Moriyama K, Sasaki Y, Ohashi K, Sekine-Aizawa Y, Sehara-Fujisawa A, Mizuno K, Goshima Y, Yahara I (2001) Phosphorylation of cofilin by LIM-kinase is necessary for semaphorin 3A-induced growth cone collapse. *Nat Neurosci* **4**, 367-373.
- [26] Yuen EY, Yan Z (2009) Dopamine D4 receptors regulate AMPA receptor trafficking and glutamatergic transmission in GABAergic interneurons of prefrontal cortex. *J Neurosci* **29**, 550-562.
- [27] Duffney LJ, Zhong P, Wei J, Matas E, Cheng J, Qin L, Ma K, Dietz DM, Kajiwara Y, Buxbaum JD, Yan Z (2015) Autism-like deficits in *Shank3*-deficient mice are rescued by targeting actin regulators. *Cell Reports* **11**, 1400-1413.
- [28] Graziane NM, Yuen EY, Yan Z (2009) Dopamine D4 receptors regulate GABA_A receptor trafficking and function via an actin/cofilin/myosin-dependent mechanism. *J Biol Chem* **284**, 8329-8336.
- [29] Yuen EY, Wei J, Liu W, Zhong P, Li X, Yan Z (2012) Repeated stress causes cognitive impairment by suppressing glutamate receptor expression and function in prefrontal cortex. *Neuron* **73**, 962-977.
- [30] Wei J, Yuen EY, Liu W, Li X, Zhong P, Karatsoreos IN, McEwen BS, Yan Z (2014) Estrogen protects against the detrimental effects of repeated stress on glutamatergic transmission and cognition. *Mol Psychiatry* **19**, 588-598.
- [31] Yuen EY, Liu W, Karatsoreos IN, Feng J, McEwen BS, Yan Z (2009) Acute stress enhances glutamatergic transmission in prefrontal cortex and facilitates working memory. *Proc Natl Acad Sci U S A* **106**, 14075-14079.
- [32] Yuen EY, Liu W, Karatsoreos IN, Ren Y, Feng J, McEwen BS, Yan Z (2011) Mechanisms for acute stress-induced enhancement of glutamatergic transmission and working memory. *Mol Psychiatry* **16**, 156-170.
- [33] Bevins RA, Besheer J (2006) Object recognition in rats and mice: A one-trial non-matching-to-sample learning task to study 'recognition memory'. *Nat Protoc* **1**, 1306-1311.
- [34] Lo CY, Wang PN, Chou KH, Wang J, He Y, Lin CP (2010) Diffusion tensor tractography reveals abnormal topological organization in structural cortical networks in Alzheimer's disease. *J Neurosci* **30**, 16876-16885.
- [35] Rosenmund C, Westbrook GL (1993) Calcium-induced actin depolymerization reduces NMDA channel activity. *Neuron* **10**, 805-814.
- [36] Allison DW, Gelfand VI, Spector I, Craig AM (1998) Role of actin in anchoring postsynaptic receptors in cultured hippocampal neurons: Differential attachment of NMDA versus AMPA receptors. *J Neurosci* **18**, 2423-2436.
- [37] Rocca DL, Martin S, Jenkins EL, Hanley JG (2008) Inhibition of Arp2/3-mediated actin polymerization by PICK1 regulates neuronal morphology and AMPA receptor endocytosis. *Nat Cell Biol* **10**, 259-271.
- [38] Fukazawa Y, Saitoh Y, Ozawa F, Ohta Y, Mizuno K, Inokuchi K (2003) Hippocampal LTP is accompanied by enhanced F-actin content within the dendritic spine that is essential for late LTP maintenance *in vivo*. *Neuron* **38**, 447-460.
- [39] Mendoza-Naranjo A, Gonzalez-Billault C, Maccioni RB (2007) Abeta1-42 stimulates actin polymerization in hippocampal neurons through Rac1 and Cdc42 Rho GTPases. *J Cell Sci* **120**, 279-288.
- [40] Henriques AG, Vieira SI, da Cruz E, Silva EF, da Cruz E, Silva OA (2010) Abeta promotes Alzheimer's disease-like cytoskeleton abnormalities with consequences to APP processing in neurons. *J Neurochem* **113**, 761-771.
- [41] Morishita W, Marie H, Malenka RC (2005) Distinct triggering and expression mechanisms underlie LTD of AMPA and NMDA synaptic responses. *Nat Neurosci* **8**, 1043-1050.
- [42] Duffney LJ, Wei J, Cheng J, Liu W, Smith KR, Kittler JT, Yan Z (2013) Shank3 deficiency induces NMDA receptor hypofunction via an actin-dependent mechanism. *J Neurosci* **33**, 15767-15778.
- [43] Aarts M, Liu Y, Liu L, Besshoh S, Arundine M, Gurd JW, Wang YT, Salter MW, Tymianski M (2002) Treatment of ischemic brain damage by perturbing NMDA receptor-PSD-95 protein interactions. *Science* **298**, 846-850.
- [44] Borsello T, Clarke PG, Hirt L, Vercelli A, Repici M, Schorderet DF, Bogousslavsky J, Bonny C (2003) A peptide inhibitor of c-Jun N-terminal kinase protects against excitotoxicity and cerebral ischemia. *Nat Med* **9**, 1180-1186.
- [45] Goldman-Rakic PS (1995) Cellular basis of working memory. *Neuron* **14**, 477-485.
- [46] Wang M, Yang Y, Wang CJ, Gamo NJ, Jin LE, Mazer JA, Morrison JH, Wang XJ, Arnsten AF (2013) NMDA receptors subserve persistent neuronal firing during working memory in dorsolateral prefrontal cortex. *Neuron* **77**, 736-749.
- [47] Mitchell JB, Laiacona J (1998) The medial frontal cortex and temporal memory: Tests using spontaneous exploratory behaviour in the rat. *Behav Brain Res* **97**, 107-113.
- [48] Ennaceur A, Delacour J (1998) A new one-trial test for neurobiological studies of memory in rats. 1: Behavioral data. *Behav Brain Res* **31**, 47-59.
- [49] Dix SL, Aggleton JP (1999) Extending the spontaneous preference test of recognition: Evidence of object-location and object-context recognition. *Behav Brain Res* **99**, 191-200.
- [50] Stokin GB, Lillo C, Falzone TL, Brusch RG, Rockenstein E, Mount SL, Raman R, Davies P, Masliah E, Williams DS, Goldstein LS (2005) Axonopathy and transport defects early in the pathogenesis of Alzheimer's disease. *Science* **307**, 1282-1288.

- [51] Davis RC, Marsden IT, Maloney MT, Minamide LS, Podlisny M, Selkoe DJ, Bamberg JR (2011) Amyloid beta dimers/trimers potently induce cofilin-actin rods that are inhibited by maintaining cofilin-phosphorylation. *Mol Neurodegener* **6**, 10.
- [52] Bamberg JR, Wiggan O (2002) ADF/cofilin and actin dynamics in disease. *Trends Cell Biol* **12**, 598-605.
- [53] Yuen EY, Liu W, Kafri T, van Praag H, Yan Z (2010) Regulation of AMPA receptor channels and synaptic plasticity by cofilin phosphatase Slingshot in cortical neurons. *J Physiol* **588**, 2361-2371.
- [54] McGough A, Pope B, Chiu W, Weeds A (1997) Cofilin changes the twist of F-actin: Implications for actin filament dynamics and cellular function. *J Cell Biol* **138**, 771-781.
- [55] Pollard TD, Borisy GG (2003) Cellular motility driven by assembly and disassembly of actin filaments. *Cell* **112**, 453-465.
- [56] Andrianantoandro E, Pollard TD (2006) Mechanism of actin filament turnover by severing and nucleation at different concentrations of ADF/cofilin. *Mol Cell* **24**, 13-23.
- [57] Niwa R, Nagata-Ohashi K, Takeichi M, Mizuno K, Uemura T (2002) Control of actin reorganization by Slingshot, a family of phosphatases that dephosphorylate ADF/cofilin. *Cell* **108**, 233-246.
- [58] Woo JA, Jung AR, Lakshmana MK, Bedrossian A, Lim Y, Bu JH, Park SA, Koo EH, Mook-Jung I, Kang DE (2012) Pivotal role of the RanBP9-cofilin pathway in A β -induced apoptosis and neurodegeneration. *Cell Death Differ* **19**, 1413-1423.
- [59] Lakshmana MK, Chung JY, Wickramarachchi S, Tak E, Bianchi E, Koo EH, et al. (2010) A fragment of the scaffolding protein RanBP9 is increased in Alzheimer's disease brains and strongly potentiates amyloid-beta peptide generation. *FASEB J* **24**, 119-127.
- [60] Woo JA, Boggess T, Uhlir C, Wang X, Khan H, Cappos G, Joly-Amado A, De Narvaez E, Majid S, Minamide LS, Bamberg JR, Morgan D, Weeber E, Kang DE (2015) RanBP9 at the intersection between cofilin and A β pathologies: Rescue of neurodegenerative changes by RanBP9 reduction. *Cell Death Dis* **6**, 1676.
- [61] Woo JA, Zhao X, Khan H, Penn C, Wang X, Joly-Amado A, Weeber E, Morgan D, Kang DE (2015) Slingshot-Cofilin activation mediates mitochondrial and synaptic dysfunction via A β ligation to β 1-integrin conformers. *Cell Death Differ* **22**, 921-934.